A&A 556, A30 (2013)
DOI: 10.1051/0004-6361/201321248

Astronomy & Astrophysics

XMM-Newton and *Swift* observations of XTE J1743-363⋆

E. Bozzo[1], P. Romano[2], C. Ferrigno[1], S. Campana[3], M. Falanga[4], G. Israel[5], R. Walter[1], and L. Stella[5]

[1] ISDC Data Centre for Astrophysics, department of Astronomy, University of Geneva, Chemin d'Écogia 16, 1290 Versoix, Switzerland
e-mail: enrico.bozzo@unige.ch
[2] INAF, Istituto di Astrofisica Spaziale e Fisica Cosmica – Palermo, via U. La Malfa 153, 90146 Palermo, Italy
[3] INAF – Osservatorio Astronomico di Brera, via Bianchi 46, 23807 Merate (LC), Italy
[4] International Space Science Institute (ISSI) Hallerstrasse 6, 3012 Bern, Switzerland
[5] INAF – Osservatorio Astronomico di Roma, via Frascati 33, 00044 Roma, Italy

Received 6 February 2013 / Accepted 6 June 2013

ABSTRACT

XTE J1743-363 is a poorly known hard X-ray transient, which displays short and intense flares similar to those observed from supergiant fast X-ray transients. The probable optical counterpart shows spectral properties similar to those of an M8 III giant, thus suggesting that XTE J1743-363 belongs to the class of the symbiotic X-ray binaries class. In this paper we report on the first dedicated monitoring campaign of the source in the soft X-ray range with *XMM-Newton* and *Swift*/XRT. These observations confirmed the association of XTE J1743-363 with the previously suggested M8 III giant and the classification of the source as a member of the symbiotic X-ray binaries. In the soft X-ray domain, XTE J1743-363 displays a high absorption ($\sim 6 \times 10^{22}$ cm^{-2}) and variability on time scales of hundreds to few thousand seconds, typical of wind-accreting systems. A relatively faint flare (peak X-ray flux 3×10^{-11} erg/cm^2/s) lasting ∼4 ks is recorded during the *XMM-Newton* observation and interpreted in terms of the wind accretion scenario.

Key words. X-rays: binaries – X-rays: individuals: XTE J1743-363

1. Introduction

XTE J1743-363 was discovered by Markwardt et al. (1999) during RXTE monitoring observations of the Galactic-center region. At that time, the source was detected undergoing episodes of enhanced X-ray activity, reaching fluxes of 15 mCrab and showing variability with time scales as short as ∼1 min. The source was also observed undergoing intense short outbursts with INTEGRAL and was thus classified as a possible supergiant fast X-ray transient (SFXT, see, e.g., Sguera et al. 2006). The brightest outburst from the source observed with INTEGRAL reached about 40 mCrab in the 20–60 keV energy band and lasted ∼2.5 h. Before the present work, XTE J1743-363 was not studied with focusing X-ray telescopes in the soft X-ray domain (0.3–12 keV) and the position of the source could be securely measured only with an accuracy of a few arcmin. A possible sub-arcmin localization of the source was proposed by Ratti et al. (2010) using an archival *Chandra* observation. In those data, about 11 photons were serendipitously recorded from a location in the relatively large INTEGRAL error circle around the position of XTE J1743-363. Based on this, Smith et al. (2012) proposed a probable optical counterpart that displays typical spectral characteristics of an M8III giant, suggesting that XTE J1743-363 could be a new member of the symbiotic X-ray binary (SyXB) class rather than an SFXT (though some uncertainties still prevent a firm conclusion about the precise spectral type of the companion). Smith et al. (2012) also reported a complete re-analysis of all RXTE/PCA data of the source and showed that its X-ray flux has continuously decreased during the past ∼13 yrs. Such a behavior was not observed before in an SFXT.

⋆ Table 2 is available in electronic for at http://www.aanda.org

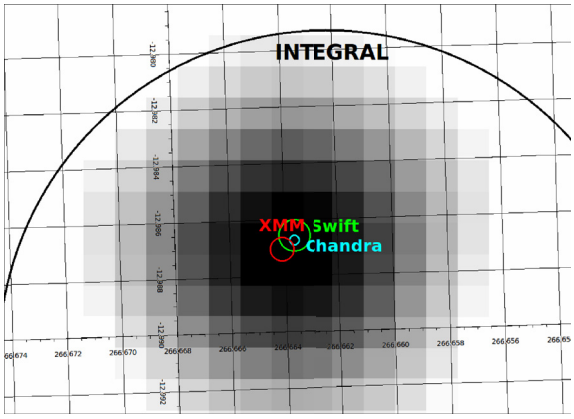

Fig. 1. Refined XMM position (1.5″ at 68% c.l.) of the source reported in the present work is compatible with the *Chandra* position of the faint source detected by Ratti et al. (0.6″ at 90% c.l.; 2010) and is suggested to be the quiescent counterpart to XTE J1743-363. We also show the INTEGRAL position (0.7′ at 90% c.l.; Bird et al. 2010) and the *Swift*/XRT position (2.3″ at 90% c.l.; see Sect. 3).

We report in this paper on the first pointed observations of XTE J1743-363 with focusing X-ray instruments. These include a deep pointing with *XMM-Newton* (total exposure time 42 ks) and a three-month-long monitoring campaign performed with *Swift*/XRT (total on-source exposure time 79 ks).

2. *XMM-Newton* data analysis and results

Starting on 2012 February 29 18:31 UT, *XMM-Newton* observed XTE J1743-363 for about 42 ks. The EPIC-pn was operated in full-frame, the EPIC-MOS1 in small window, and the

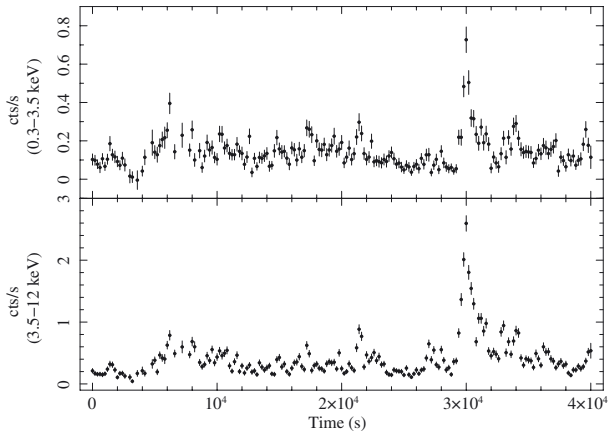

Fig. 2. EPIC-pn lightcurve of XTE J1743-363 in the 0.3–3.5 keV (*upper panel*) and 3.5–12 keV (*lower panel*) energy band. The start time is 55 986.8017 MJD and the bin time is 200 s.

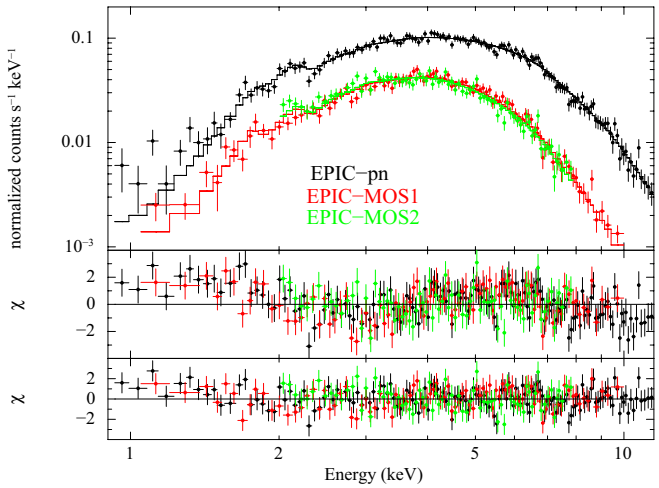

Fig. 3. EPIC-pn (black), EPIC-MOS1 (red), and EPIC-MOS2 (green) spectra of XTE J1743-363 extracted by using the entire exposure time available from the *XMM-Newton* observation. The best fit is obtained here with an absorbed BMC model. The residuals from this fit are shown in the *bottom panel*. The *middle panel* shows the residuals from a fit with a simple power-law model.

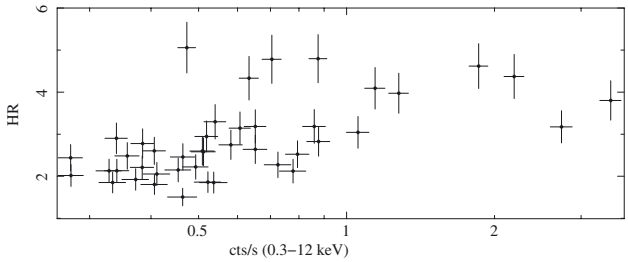

Fig. 4. HID of the source realized by using the same lightcurves shown in Fig. 2 adaptively rebinned to a $S/N = 9$ (see also Fig. 5).

MOS2 in timing mode. Observation data files (ODFs) were processed to produce calibrated event lists using the standard *XMM-Newton* Science Analysis System (v. 12.0.1). We used the EPPROC and EMPROC tasks to produce cleaned event files from the Epic-pn and MOS cameras, respectively. The Epic-pn and Epic-MOS event files were filtered in the 0.3–12 keV and 0.5–10 keV energy range, respectively. High background time intervals were excluded using standard techniques[1]. The effective exposure time was 33 ks for the EPIC-pn and 40 ks for the MOS cameras. Lightcurves and spectra of the source and background were extracted by using regions in the same CCD for the MOS and from adjacent CCDs at the same distance to the readout node for the EPIC-pn[2]. The difference in extraction areas between source and background was accounted for by using the SAS BACKSCALE task for the spectra and LCCORRR for the lightcurves. All EPIC spectra were rebinned before fitting in order to have at least 15–25 counts per bin (depending on the statistics of each spectrum) and, at the same time, prevent oversampling of the energy resolution by more than a factor of three. Where required, we barycenter-corrected the photon arrival times in the EPIC event files with the *barycen* tool. Throughout this paper, uncertainties are given at 90% c.l., unless stated otherwise. The best position of XTE J1743-363 determined by the EPIC-pn and MOS1 is at $\alpha_{J2000} = 17^{h}43^{m}01\overset{s}{.}44$ and $\delta_{J2000} = -36°22'23\overset{''}{.}16$, with an associated uncertainty of 1.5 arcsec. at 68% c.l.[3]. In Fig. 2 we show the EPIC-pn background-subtracted source lightcurve in two energy bands. A flare from the source is observed about 30 ks after the beginning of the observation. The averaged EPIC-pn, MOS1, and MOS2 spectra of the observation are shown in Fig. 3. A simultaneous fit to all spectra[4] with a simple absorbed power-law model gave an absorption column density $N_{H} = (6.1 \pm 0.2) \times 10^{22}$ cm^{-2}, a photon index $\Gamma = 1.51 \pm 0.05$, and a poor χ^2_{red}/d.o.f. = 1.34/314. The observed 2–10 keV X-ray flux was 5.7×10^{-12} erg/cm^2/s. In order to improve the fit, we first considered a bulk motion Comptonization (BMC) model, which accounts for the soft thermal emission from the neutron star and its Comptonization in a self-consistent way (Titarchuk et al. 1997). We then tried a model comprising a MEKAL (i.e., emission from a thin thermal medium) and a power-law component (see discussion in Bozzo et al. 2010). The BMC model provided a statistically acceptable fit (see Table 1), but only an upper limit could be obtained on the spectral index parameter $\alpha = \Gamma - 1$. This is due to the limited energy coverage of the *XMM-Newton* spectra (0.3–12 keV). Other spectral models with similar numbers of free parameters, including a cut-off power-law or a power-law with an exponential rollover, also provided reasonably good fits to the data. However, these models gave very low value of the cut-off and exponential rollover energies (~4 keV) and unlikely negative power-law photon indices ($\Gamma \sim -0.5$). We checked a posteriori that different choices of the energy binning and background extraction region would not affect these results.

In order to study possible spectral variations during the observation, we extracted the hardness-intensity diagram (HID) of the source (this was calculated as in our previous papers, see, e.g., Bozzo et al. 2010). From Fig. 4 we noticed that the hardness ratio (HR) could not be easily related to changes of the source overall intensity. To better investigate the behavior of the HR, we rebinned the source lightcurve adaptively in order to have in each

[1] http://xmm.esac.esa.int/sas/current/documentation/threads/EPIC_filterbackground.shtml.

[2] See http://xmm.esac.esa.int/sas/current/documentation/threads.

[3] See http://xmm.esac.esa.int/sas/current/documentation/threads/src_find_thread.shtml and http://xmm2.esac.esa.int/docs/documents/CAL-TN-0018.ps.gz.

[4] The EPIC-MOS2 spectrum (operated in timing mode) showed evident instrumental residuals below 2.0 keV and above 8.0 keV, not present in the other spectra of the source. These data were thus discarded for further analysis.

Table 1. Simultaneous fit to the EPIC-pn, MOS1, and MOS2 spectra of the entire observation and the time intervals displayed in the bottom panel of Fig. 5.

Model	$N_{\rm H}$	Γ	kT	$N_{\rm mekal}$	$\log A$	$N_{\rm BMC}$	$F_{\rm X}$	$C_{\rm MOS1}$	$C_{\rm MOS2}$	$\chi^2_{\rm red}$/d.o.f.
Tot.										
ph*BMC	3.57 ± 0.17	<2.5	$1.45^{+0.06}_{-0.07}$	–	$2.17^{+0.10}_{-0.12}$	$(8.3^{+0.9}_{-0.7}) \times 10^{-3}$	5.6	1.05 ± 0.03	1.10 ± 0.02	1.04/312
ph*(mkl+pl)	7.0 ± 0.3	1.66 ± 0.06	$0.113^{+0.043}_{-0.003}$	$68.1^{+107.8}_{-54.4}$	–	–	5.7	1.04 ± 0.03	1.11 ± 0.03	1.14/312
Spectrum "a"										
ph*pl	5.6 ± 0.3	1.63 ± 0.07	–	–	–	–	4.3	1.06 ± 0.04	1.17 ± 0.04	1.26/281
ph*BMC	3.2 ± 0.2	<2.5	$1.34^{+0.07}_{-0.09}$	–	$2.15^{+0.11}_{-0.15}$	$(5.5^{+0.2}_{-0.8}) \times 10^{-3}$	4.3	$1.06^{+0.02}_{-0.04}$	1.17 ± 0.04	1.10/279
ph*(mkl+pl)	6.2 ± 0.4	1.73 ± 0.08	$0.112^{+0.050}_{-0.05}$	$32.5^{+64.2}_{-31.5}$	–	–	4.3	1.06 ± 0.04	1.18 ± 0.04	1.15/279
Spectrum "b"										
ph*pl	$11.3^{+2.0}_{-1.7}$	1.8 ± 0.3	–	–	–	–	5.1	1.11 ± 0.13	1.12 ± 0.14	1.02/69
ph*BMC	$7.8^{+1.7}_{-1.4}$	2.5 (fixed)	1.2 ± 0.2	–	2.17 (fixed)	$(9.9^{+0.9}_{-0.8}) \times 10^{-5}$	5.0	1.11 ± 0.12	1.13 ± 0.14	0.97/69
Spectrum "c"										
ph*pl	$7.9^{+3.9}_{-3.5}$	1.1 ± 0.5	–	–	–	–	21.7	1.0 ± 0.2	1.0 ± 0.2	0.76/31
ph*BMC	$4.6^{+3.4}_{-2.8}$	2.5 (fixed)	$1.8^{+0.5}_{-0.7}$	–	2.17 (fixed)	$(4.7^{+2.1}_{-1.0}) \times 10^{-4}$	21.2	1.0 ± 0.2	1.0 ± 0.2	0.75/31
Spectrum "d"										
ph*pl	$6.5^{+1.3}_{-1.1}$	1.1 ± 0.2	–	–	–	–	30.7	1.1 ± 0.1	1.1 ± 0.1	1.00/90
ph*BMC	$4.1^{+1.0}_{-0.8}$	2.5 (fixed)	$1.7^{+0.3}_{-0.2}$	–	2.17 (fixed)	$(6.4^{+1.0}_{-0.8}) \times 10^{-4}$	30.0	1.1 ± 0.1	1.1 ± 0.1	0.95/90
Spectrum "e"										
ph*pl	7.8 ± 1.0	1.3 ± 0.2	–	–	–	–	13.5	1.1 ± 0.1	1.1 ± 0.1	0.89/105
ph*BMC	$5.2^{+0.8}_{-0.7}$	2.5 (fixed)	1.5 ± 0.2	–	2.17 (fixed)	$(2.7^{+0.3}_{-0.2}) \times 10^{-4}$	13.1	1.1 ± 0.1	1.1 ± 0.1	0.89/105
Spectrum "f"										
ph*pl	7.1 ± 0.5	1.8 ± 0.1	–	–	–	–	5.7	1.05 ± 0.06	1.12 ± 0.07	1.16/189
ph*BMC	$4.5^{+0.5}_{-0.4}$	2.5 (fixed)	1.15 ± 0.08	–	2.17 (fixed)	$(9.5 \pm 0.4) \times 10^{-5}$	5.7	1.05 ± 0.06	1.12 ± 0.07	1.12/189

Notes. We indicated above with "ph", "mkl", "BB", and "pl" the PHABS, MEKAL, BLACKBODY, and power-law component of the spectral model used in XSPEC. In the BMC model $\alpha = \Gamma - 1$ is the energy spectral index, $\log A$ gives a measurement of the fraction of the Compton-reprocessed emission with respect to the directly observed blackbody emission, and $N_{\rm BMC}$ can be used to estimate the size of the thermally emitting region (see also Sect. 4). We did not explicitly report the normalization of the power-law component in the ph*pl, as this parameter would not provide additional information beside the source flux already given in the fourth column on the right). $C_{\rm MOS1}$ and $C_{\rm MOS2}$ are the normalization constants introduced in the model to account for inter-calibration uncertainties between the EPIC cameras ($C = 1$ for the EPIC-pn). The absorption column density reported here is given in units of 10^{22} cm^{-2}, kT in keV, and the flux in units of 10^{-12} erg/cm^2/s (2–10 keV energy range, not corrected for absorption).

bin a signal-to-noise ratio (S/N) of 9. This is shown in Fig. 5. The complex behavior of the source HR is especially puzzling shortly before until after the bright flare occurring at $t \sim 30$ ks from the beginning of the observation. In particular, it is evident that the HR significantly increases about 3 ks before the peak of the flare, displays a sudden drop of few hundred seconds immediately after the peak, and then decreases back to the value of the first part of the observation (showing similar but less pronounced variations). We investigated the origin of this variability by dividing the total observation into six time intervals (see Fig. 5) and performing a time-resolved spectral analysis. The EPIC-pn and EPIC-MOS spectra extracted during the same time intervals were fit together to increase the statistics and thus reduce the uncertainties in the fit parameters. Given the shorter exposure times and lower statistics with respect to the spectrum of the entire observation, all time-resolved spectra could be well fit by using a simple power-law model (the only exception being the spectrum "a", which has the longest exposure time). For consistency with the results obtained from the total spectrum, we also fit the time resolved spectra with the BMC model (we fixed in most cases the value of $\log(A)$ and α as these parameters could not be constrained). The results are given in Table 1 and shown in Fig. 5. The fits to the time-resolved spectra with all models suggest there was a significant change in the spectral parameters during the bright flare. The largest variation occurs between the time intervals "b" and "d". To demonstrate that these changes are not model dependent, we also show in Fig. 6 the contour plots of the spectral parameters of the absorbed BMC and the power-law model, which displayed a significant change during these intervals. We note that the variation of the $N_{\rm H}$ revealed from the fit with a simple absorbed power-law model is fully consistent with the ph*(mkl+pl) interpretation of the X-ray spectrum. During the time passed from the "b" to the "d" time intervals ($\lesssim$1.5 ks) we would not expect significant changes in the MEKAL component, as the latter should not vary on timescales shorter than $R_{\rm mekal}/c \sim 2.3$ ks (here c is the speed of light and $R_{\rm mekal} > 10^{13}$ cm, as estimated in Sect. 4). We verified that the addition of a MEKAL component with temperature and normalization fixed to the values determined from the total spectrum to the time-resolved spectra would not significantly affect the results presented in Fig. 6.

The results in Figs. 5 and 6 suggest that the absorption column density in the direction of the source rose up about 3 ks before the onset of the flare, dropped close to the peak of the event (when the source reached the highest X-ray flux), and then rose again during the initial decay of the flare. Correspondingly, we observed a flattening of the power-law photon index (in the fit with the model ph*pl) or an increase in the temperature of

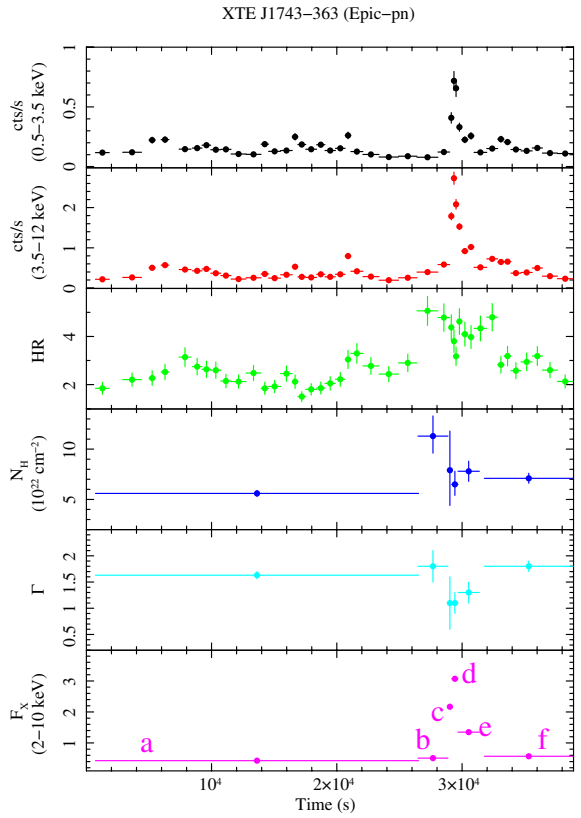

Fig. 5. First two panels from the top show the source lightcurves of Fig. 2 rebinned adaptively to a $S/N = 9$ (based on the lightcurve in the 0.3–3.5 keV energy band). The third panel from the top shows the HR, calculated as the ratio between the source count-rate in the 3.5–12 keV vs. count-rate in the 0.3–3.5 keV energy band. The other three panels show the absorption column density (N_H), the power-law photon index (Γ), and the observed flux (units of 10^{-11} erg/cm^2/s) in different time intervals as revealed from our time-resolved spectral analysis (see text for details).

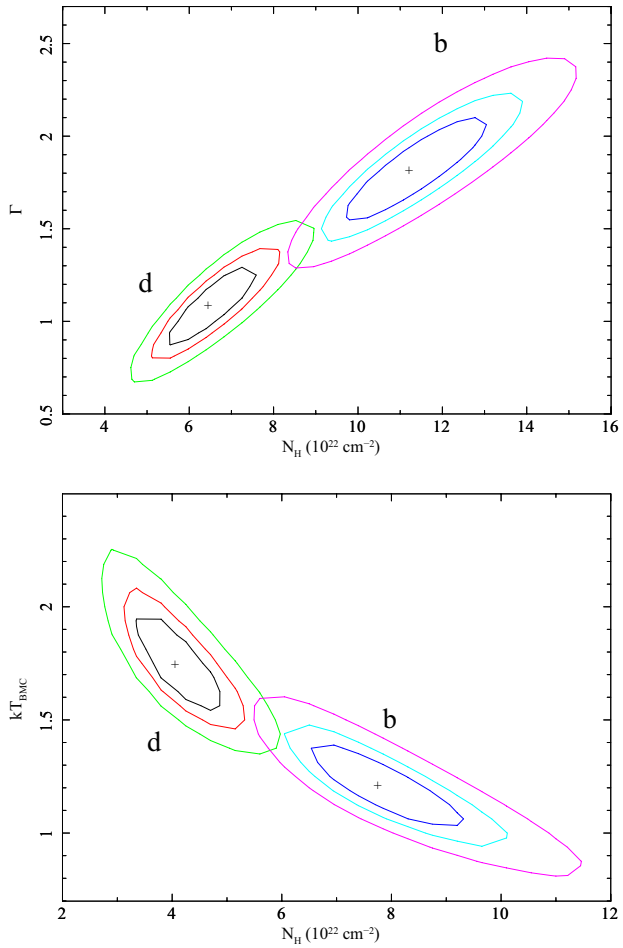

Fig. 6. Contours plot (68%, 90%, and 99% c.l.) obtained from the fit to the spectra "b" and "d" with the ph*pl and ph*BMC models (see Fig. 5 and Table 1).

the seed thermal photons in the fit with the ph*BMC model. The interpretation of these results is discussed in Sect. 4. We note that fixing the same value of the absorption column density measured for spectrum "d" in the fit to the spectrum "b" would give unacceptable results in both cases of the ph*pl and ph*BMC models (χ^2_{red}/d.o.f. = 1.41/70 and 1.37/70, respectively). The same conclusion applies if the absorption column density measured for spectrum "b" is used and fixed in the fit to the spectrum "d". In this case we obtained for the ph*pl and ph*BMC models χ^2_{red}/d.o.f. = 1.30/91 and 1.23/91, respectively.

The source and background EPIC MOS and pn event lists were used to carry out an in-depth search for coherent signals after barycenter correction. We applied the power-spectrum search algorithm developed by Israel & Stella (1996) to the lists of barycentered photon arrival times. This method is optimized to search for periodicities in "colored" power spectrum components and provides upper limits if no signal is detected. Due to the different sampling times of the three EPIC cameras we decided to carry out the search in three different ways: (i) by using all the event lists and a binning time of 0.3 s, (ii) by combining the MOS2 and pn event lists with binning time of 73.4 ms (keeping the original Fourier resolution); and (iii) by using only the MOS2 event list with a binning time of 1.75 ms (thus maximizing the Nyquist frequency). No significant signal was found. We show in Fig. 7 the derived 3σ upper limits to the pulsed fraction as a function of the pulse frequency.

3. *Swift* data analysis and results

The *Swift* X-ray telescope (XRT, Burrows et al. 2005) data data were obtained as a target of opportunity (ToO) monitoring campaign. The ToO started on 2012 April 19 with 1 ks per day until July 20; then 1 ks observations were carried out every other day. The campaign lasted 115 days, with 82 observations for a total on-source exposure of 79 ks. We also considered the archival *Swift* observation 00037884001 from 2010 February (see Table 2 for details).

The XRT data were processed with standard procedures (XRTPIPELINE v0.12.6), and filtering and screening criteria were applied by using FTOOLS in the HEASOFT package (v.6.12). Given the low count rate of the source throughout the monitoring campaign, we only considered photon-counting (PC) mode data, and selected event grades 0–12 (Burrows et al. 2005). We used the latest spectral redistribution matrices in CALDB (20120713). The best source position determined with XRT is at $\alpha_{J2000} = 17^h43^m01\overset{s}{.}31$ and $\delta_{J2000} = -36°22'21\overset{''}{.}4$, with an associated uncertainty of 2.3″ at 90% c.l.[5].

The 0.3–10 keV XRT background-subtracted lightcurve was created at a 1 day resolution and shown in Fig. 8. All count-rate measurements have been corrected for point spread function (PSF) losses and vignetting. The source could not be detected in

[5] We used the online tool http://www.swift.ac.uk/user_objects/; see Evans et al. (2009).

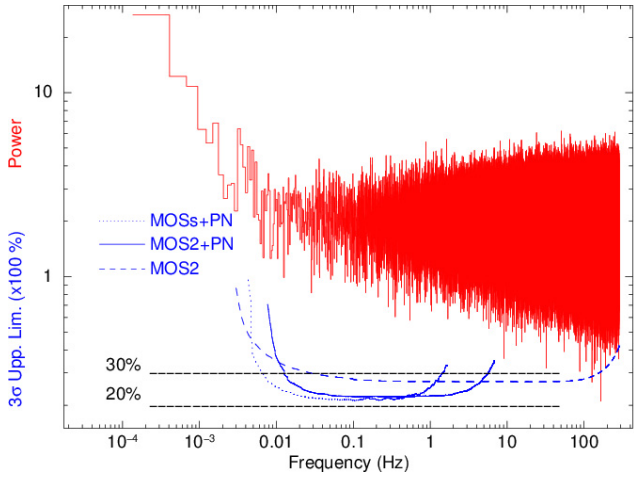

Fig. 7. In the upper part of the plot we show the power spectrum produced using the MOS2 event list as an example. In the bottom part of the plot we show the curves representing the upper limits to the non-detection of pulsations calculated according to Israel & Stella (1996). The solid, dashed and dotted lines correspond to the different sampling times and event list combinations discussed in the text. The two horizontal dashed lines represent the 20% and 30% upper limit levels on the pulsed fraction upper limits as a function of the frequency. The most stringent upper limits we could provide are at 20–30% for frequencies in the range 0.005–200 Hz.

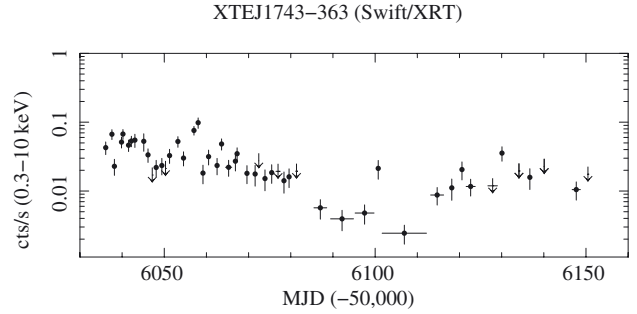

Fig. 8. Long-term monitoring of XTE J1743-363 performed with *Swift*/XRT (the campaign started about 50 days after the *XMM-Newton* observation). The count-rate is given in the 0.3–10 keV energy range. Assuming the source averaged spectral properties reported in Sect. 3, a count-rate of 0.01 cts/s corresponds to about 1.2×10^{-12} erg/cm^2/s. Downward arrows correspond to 3σ upperlimits on the source count-rate.

all observations. In order to preserve a good sampling in time for the source count-rate, we stacked together close-by observations in which a detection of the source could not be obtained after a few days of integration (∼2–3). For all isolated non-detections, we indicated in the figure the corresponding 3σ upperlimits on the source count-rate with downward arrows. We did not include in Fig. 8 the observation 00037884001. At the epoch of this observation, XRT did not detect the source and we derived a 90% c.l. upper limit on its X-ray flux of 8×10^{-13} erg/cm^2/s (2–10 keV not corrected for absorption). This is the only observation in the soft X-ray domain that overlaps with previously reported RXTE data (see Sect. 4).

For our spectral analysis, we extracted the mean spectrum in the same regions as those adopted for the light curves; ancillary response files were generated with XRTMKARF to account for different extraction regions, vignetting, and PSF corrections. The data were rebinned with a minimum of 20 counts per energy bin and fit in the 0.3–10 keV energy range. The XRT spectrum (see Fig. 9) could be well fit ($\chi^2_{\rm red}$/d.o.f. = 0.90/56) with

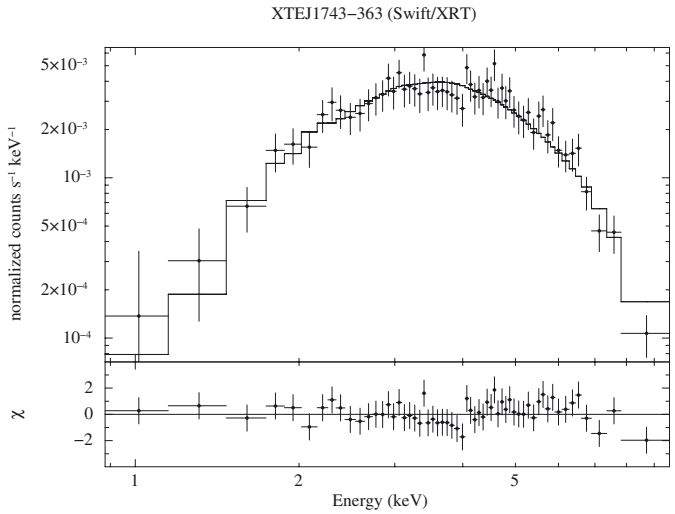

Fig. 9. *Swift*/XRT spectrum extracted by summing up all data in Table 2. The best fit is obtained with a simple absorbed power-law model (see text for details). The residuals from this fit are shown in the bottom panel.

a simple absorbed power-law model. We obtained $N_{\rm H} = (5.6 \pm 0.9) \times 10^{22}$ cm^{-2} and $\Gamma = 1.6 \pm 0.3$, which is in reasonably good agreement with the average results obtained from *XMM-Newton* (Sect. 2). The averaged observed 2–10 keV X-ray flux was 2.0×10^{-12} erg/cm^2/s. For comparison with results in Sect. 2 we also fit the XRT spectrum with the ph*BMC model ($\chi^2_{\rm red}$/d.o.f. = 0.65/56). In this case we obtained $N_{\rm H} = (3.4^{+0.8}_{-0.6}) \times 10^{22}$ cm^{-2}, $kT = 1.1 \pm 0.2$ keV, and $N_{\rm BMC} = (2.8 \pm 0.3) \times 10^{-5}$. As XRT recorded a total of only 1244 counts from the source, we did not attempt a time-resolved spectral analysis of the XRT data.

4. Discussion and conclusions

In this paper, we reported for the first time an in-depth monitoring of XTE J1743-363 in the soft X-ray domain (0.3–12 keV). The position of the source determined from these data at a few arcsec accuracy is compatible with that suggested previously by Ratti et al. (2010), thus confirming the association of XTE J1743-363 with the M8III giant star identified by Smith et al. (2012) and the classification of the source as a SyXBs.

In the *XMM-Newton* data, the source displayed variability on timescales of a few hundred to a few thousands of seconds. A relatively bright flare occurred about 30 ks after the beginning of the observation and lasted for a few ks. Such behavior is reminiscent of what is often observed in neutron star (NS) wind-accreting binaries. This conclusion is also supported by the spectral analysis. The average *XMM-Newton* spectrum could be described reasonably well with models usually adopted for wind-accreting systems. The BMC model provided the best description of the data, but reasonably good results could also be obtained by using a model comprising a thin thermal emission component and a power-law. The BMC model describes with a self-consistent approach the case in which blackbody seed photons from the NS are subjected to bulk and thermal Comptonization in an optically thin regime (Titarchuk et al. 1997). In this model the parameter $\log(A)$ gives an indication of the fraction of the Comptonized thermal photons with respect to those that are directly visible (for $\log(A) = 8$ there is no thermal emission directly visible, whereas for $\log(A) = -8$ there is no effect due to the Comptonization). From the normalization of the BMC model it is also possible to estimate the extension of

the thermal emitting region according to the equation (see, e.g., Bozzo et al. 2010, and references therein):

$$R_{\rm BMC} = \frac{88}{C^{1/2}} \frac{N_{\rm BMC}^{1/2} d_{10\ \rm kpc}}{(kT)^2_{1\ \rm keV}}\ \rm km, \quad (1)$$

where $(kT)_{1\ \rm keV}$ is the temperature of the thermal emitting component in units of 1 keV and $C = 0.25$ for an emitting surface with the geometry of a circular slab. Equation (1) and the results of the fit to the total spectrum in Table 1 (where the spectral parameters are better constrained) suggest a radius for the thermal emitting region of 1 to a few km (for a distance of ∼5 kpc; Smith et al. 2012). Such an extended "hot-spot" would be expected in the case of wind-fed systems accreting at low luminosities (see discussion in Bozzo et al. 2010, and references therein). We note that at 5 kpc the peak luminosity recorded by *XMM-Newton* from XTE J1743-363 is $\sim 10^{35}$ erg/s. As the temperature of the emitted thermal radiation is about 1–2 keV and the energy coverage of the *XMM-Newton* data is limited to 12 keV, we could not well constraint the spectral index α.

Even though the BMC model was statistically preferable, a relatively good description of the data could also be obtained by using a model comprising a power-law and a MEKAL component. The latter component accounts in this model for the excess that emerges at energies $\lesssim$2 keV when a simple absorbed power-law model is used to fit the data (see Fig. 3). Similar "soft excesses" have been found in a number of SFXT sources (Bozzo et al. 2010; Sidoli 2010), SyXBs (Masetti et al. 2006), and are thought to be a ubiquitous characteristic of all NS accreting X-ray binaries (Hickox et al. 2004). As discussed in Bozzo et al. (2010), the MEKAL component in wind-fed systems with accreting NSs might represent the contribution to the total X-ray emission from the wind of the companion star. The normalization of the MEKAL component can also be translated into an estimate of the size of the emitting region (see, e.g., Bozzo et al. 2010, and reference therein):

$$R_{\rm mekal} = \sqrt[3]{\frac{3N_{\rm mekal}}{10^{-14}} \left(\frac{d}{n_{\rm H}}\right)^2} \simeq 7 \times 10^{13} d^{2/3}_{5\ \rm kpc} a^{2/3}_{13}\ \rm cm, \quad (2)$$

where $d_{5\rm kpc}$ is the source distance in units of 5 kpc, $n_{\rm H} \sim N_{\rm H}/a$, a_{13} is the binary separation in units of 10^{13} cm, and we made use of the results in Table 1 for $N_{\rm mekal}$ and $N_{\rm H}$. This is consistent with the soft X-ray emission in XTE J1743-363 being produced in the surroundings of an NS hosted in a wide binary system. As the orbital period of XTE J1743-363 is not known, it is not presently possible to assess the applicability of this model. We remark that a similar soft spectral component was detected during a *BeppoSAX* observation of the SyXB 4U 1954+31 and interpreted in the same way (Masetti et al. 2006).

In Sect. 2 we analyzed in detail the behavior of the HR recorded during the *XMM-Newton* observation. We showed in particular that the HR underwent a clear change shortly before until after the bright flare, which was detected about 30 ks after the beginning of the observation. Our analysis showed that there was an increase of the absorption column density before the onset of the event, followed by a sudden drop at the peak of the flare for about a few hundreds of seconds. This behavior of the HR is similar to what was observed during a flare from the SFXT IGR J18410-0535, which was caught by *XMM-Newton* in 2011 (Bozzo et al. 2011). On that occasion the flare was ascribed to an episode of enhanced accretion onto the NS due to the encounter with a "clump" of material from the stellar wind. The drop in the absorption column density at the peak of the flare was interpreted as being due to the photo-ionization of the clump by X-rays from the NS. If a similar interpretation is applied to the flare from XTE J1743-363, the calculations in Bozzo et al. (2011) suggest in this case a clump radius of $R_{\rm cl} \sim 2.2 \times 10^{10} v_{\rm w7}$ cm, where we scaled the wind velocity to a value that is more appropriate for an M giant star (∼50–500 km s^{-1}; see, e.g., Espey & Crowley 2008; Lü et al. 2012, and references therein). At this low velocity, the accretion radius of the NS is $R_{\rm acc} = 2GM/v^2_{\rm w} = 3.7 \times 10^{12} v^{-2}_{\rm w7}$ cm and thus becomes larger than the estimated size of the clump[6]. At variance with the case of IGR J18410-0535, we thus cannot make use here of the equation $M_{\rm cl} = M_{\rm acc}(R_{\rm cl}/R_{\rm acc})^2$ from Bozzo et al. (2011). Instead, we have to infer the mass of the clump directly from the observation, i.e., $M_{\rm cl} \simeq M_{\rm acc}$. The latter can be estimated as $M_{\rm acc} = 9 \times 10^{17} d^2_{5\ \rm kpc}$ g by using the observed flare duration of 4.4 ks and integrating over time the unabsorbed flux measured during the intervals b, c, d, and e in Fig. 5. The absorption column density caused by the passage of this clump along the line of sight to the X-ray source is $N_{\rm H} \sim M_{\rm cl}/(R^2_{\rm cl} m_{\rm p}) \sim 10^{21} v^{-2}_{w7} d^2_{5\ \rm kpc}$ cm^{-2}, thus suggesting for XTE J1743-363 a particularly low velocity (the absorption column density measured from the *XMM-Newton* spectra is $N_{\rm H} \sim 10^{23}$ cm^{-2}, see Table 1). We note that complex accretion environments and inhomogeneous winds in SyXBs were already suggested in the case of 4U 1954+31, where an X-ray spectrum revealed the presence of multiple and variable absorbers close to the NS (Mattana et al. 2006; Masetti et al. 2006). As also mentioned for IGR J18410-0535 and other wind-accreting binaries, the NS magnetic field and rotation might also play a role regulating the amount of material that can be accumulated and accreted close to the star magnetospheric boundary (Grebenev & Sunyaev 2007; Bozzo et al. 2008; Postnov et al. 2010). The "magnetic and centrifugal gates" depend on the local condition at the NS magnetospheric boundary, in particular, on the magnetic field strength and rotation velocity of the compact object. The lack of information on the properties of the NS hosted in XTE J1743-363 and the system geometry (e.g., orbital period, eccentricity) prevent a detailed investigation on how these gates can affect the parameters of the clump reported above. Further observations of SyXBs with X-ray instruments endowed with a large collecting area in the soft X-ray domain can help investigate their flaring behavior in more detail and understand the properties of winds from cool stars. The candidate ESA mission LOFT (Feroci et al. 2012) can provide significantly better capabilities in these respects compared to the present generation of X-ray telescopes. The unprecedented large effective area of its onboard Large Area Detector (LAD), which operates in the energy range 2–30 keV, will be able to detect spectral variations during enhanced X-ray emission episodes in bright accreting binaries down to time scales of few seconds (see also discussion in Bozzo et al. 2013).

Our long-term monitoring campaign with XRT (see Sect. 3) evidenced a ∼40-day period of particularly puzzling low X-ray intensity of the source centered around 56 100 MJD (see Fig. 8). This period was interrupted only by a single flare occurring at ∼56 100 MJD (in the corresponding XRT pointing, the source displayed a count-rate of $\sim 2 \times 10^{-2}$ cts/s compared to an average count-rate of $\sim 5 \times 10^{-3}$ cts/s in the nearby observations). We note that similar low-intensity episodes were also reported previously by Smith et al. (2012), e.g., around 54 115 MJD. In some

[6] We neglected in the calculation of $R_{\rm acc}$ the contribution of the NS orbital velocity (see, e.g., Bozzo et al. 2008). For the range of system parameters (masses, orbital periods, and wind velocities) considered here for an SyXB, the NS orbital velocity would be comparable or lower than $v_{\rm w}$, thus this approximation does not significantly affect our conclusions.

of the RXTE observations, the emission recorded by the PCA from the direction of the source was compatible with being due only to Galactic diffuse emission, suggesting that in these periods XTE J1743-363 was in a quiescent state ($\ll 10^{-11}$ erg/cm^2/s). The latest available PCA observations performed toward the end of the RXTE campaign (from ~55 200 MJD to ~55 300 MJD) also caught XTE J1743-363 again in a low quiescent state (see Fig. 7 in Smith et al. 2012). The *Swift* pointing ID. 00037884001 that was carried out in the direction of the source at a similar epoch (55 237.82 MJD, see Sect. 3) did not detect any significant X-ray emission and placed a tight upper limit on its flux at 8×10^{-13} erg/cm^2/s (2–10 keV). This is compatible with the flux measured by *Swift* during the low-intensity episode that occurred around 56100 MJD. Outside these two quiescent periods, the fluxes measured by *XMM-Newton* and *Swift* are a factor of 5–10 lower than that measured during the latest RXTE observations, which still caught XTE J1743-363 undergoing some residual X-ray activity (~3×10^{-11} erg/cm^2/s) around 54 304 MJD. We thus conclude that, besides the overall decreasing trend in the source X-ray emission over the past 15 yrs (Smith et al. 2012), XTE J1743-363 also displays quiescent periods lasting several to tens of days.

Acknowledgements. We thank the anonymous referee for his/her constructive suggestions, which helped us improve the paper. P.R. acknowledges financial contribution from the contract ASI-INAF I/004/11/0. E.B. acknowledges support from ISSI through funding for the International Team on "Unified View of Stellar Winds in Massive X-ray Binaries" (leader: S. Martínez-Nuñez).

References

Bird, A. J., Bazzano, A., Bassani, L., et al. 2010, ApJS, 186, 1
Bozzo, E., Stella, L., Israel, G., Falanga, M., & Campana, S. 2008, MNRAS, 391, L108
Bozzo, E., Stella, L., Ferrigno, C., et al. 2010, A&A, 519, A6
Bozzo, E., Giunta, A., Cusumano, G., et al. 2011, A&A, 531, A130
Bozzo, E., Romano, P., Ferrigno, C., Esposito, P., & Mangano, V. 2013, Adv. Space Res., 51, 1593
Burrows, D. N., Hill, J. E., Nousek, J. A., et al. 2005, Space Sci. Rev., 120, 165
Espey, B. R., & Crowley, C. 2008, in RS Ophiuchi (2006) and the Recurrent Nova Phenomenon, eds. A. Evans, M. F. Bode, T. J. O'Brien, & M. J. Darnley, ASP Conf. Ser., 401, 166
Evans, P. A., Beardmore, A. P., Page, K. L., et al. 2009, MNRAS, 397, 1177
Feroci, M., Stella, L., van der Klis, M., et al. 2012, Exp. Astron., 34, 415
Grebenev, S. A., & Sunyaev, R. A. 2007, Astron. Lett., 33, 149
Hickox, R. C., Narayan, R., & Kallman, T. R. 2004, ApJ, 614, 881
Israel, G. L., & Stella, L. 1996, ApJ, 468, 369
Lü, G.-L., Zhu, C.-H., Postnov, K. A., et al. 2012, MNRAS, 424, 2265
Markwardt, C. B., Swank, J. H., & Marshall, F. E. 1999, IAU Circ., 7120, 1
Masetti, N., Orlandini, M., Palazzi, E., Amati, L., & Frontera, F. 2006, A&A, 453, 295
Mattana, F., Götz, D., Falanga, M., et al. 2006, A&A, 460, L1
Postnov, K., Shakura, N., González-Galán, A., et al. 2010, in Eighth Integral Workshop. The Restless Gamma-ray Universe (INTEGRAL 2010)
Ratti, E. M., Bassa, C. G., Torres, M. A. P., et al. 2010, MNRAS, 408, 1866
Sguera, V., Bazzano, A., Bird, A. J., et al. 2006, ApJ, 646, 452
Sidoli, L. 2010, AIP Conf. Proc., 1314, 271
Smith, D. M., Markwardt, C. B., Swank, J. H., & Negueruela, I. 2012, MNRAS, 422, 2661
Titarchuk, L., Mastichiadis, A., & Kylafis, N. D. 1997, ApJ, 487, 834

Pages 8 to 9 are available in the electronic edition of the journal at http://www.aanda.org

Table 2. Summary of all *Swift* /XRT pointings used in this paper.

Sequence	Obs/Mode	Start time (UT) (yyyy-mm-dd hh:mm:ss)	End time (UT) (yyyy-mm-dd hh:mm:ss)	Exposure (s)
00037884001	XRT/PC	2010-02-10 19:41:08	2010-02-10 23:12:56	2873
00037884002	XRT/PC	2012-04-19 02:43:56	2012-04-19 02:59:57	938
00037884004	XRT/PC	2012-04-20 14:03:38	2012-04-20 14:20:56	1018
00037884005	XRT/PC	2012-04-21 02:50:05	2012-04-21 05:49:56	1151
00037884006	XRT/PC	2012-04-22 20:29:17	2012-04-22 20:46:58	1051
00037884007	XRT/PC	2012-04-23 04:34:20	2012-04-23 04:51:58	1038
00037884008	XRT/PC	2012-04-24 12:35:18	2012-04-24 12:52:56	1056
00037884009	XRT/PC	2012-04-25 03:12:18	2012-04-25 06:32:57	1096
00037884010	XRT/PC	2012-04-26 00:03:19	2012-04-26 01:51:57	634
00037884011	XRT/PC	2012-04-27 03:14:23	2012-04-27 03:30:56	970
00037884012	XRT/PC	2012-04-28 03:19:23	2012-04-28 03:35:56	396
00037884013	XRT/PC	2012-04-29 03:19:19	2012-04-29 03:36:57	1038
00037884014	XRT/PC	2012-04-30 03:26:24	2012-04-30 03:43:57	1033
00037884015	XRT/PC	2012-05-01 01:53:25	2012-05-01 02:11:58	1101
00037884016	XRT/PC	2012-05-02 09:54:42	2012-05-02 10:11:58	1033
00037884017	XRT/PC	2012-05-03 06:52:10	2012-05-03 07:09:56	1043
00037884018	XRT/PC	2012-05-04 05:19:54	2012-05-04 07:00:56	1008
00037884020	XRT/PC	2012-05-06 05:28:38	2012-05-06 05:46:56	1098
00037884021	XRT/PC	2012-05-07 13:32:18	2012-05-07 13:50:57	1101
00037884022	XRT/PC	2012-05-10 00:45:16	2012-05-10 01:02:57	1058
00037884023	XRT/PC	2012-05-11 00:45:10	2012-05-11 01:02:56	1046
00037884024	XRT/PC	2012-05-12 04:02:13	2012-05-12 04:19:56	1048
00037884025	XRT/PC	2012-05-13 12:09:11	2012-05-13 12:26:56	1048
00037884026	XRT/PC	2012-05-14 00:59:08	2012-05-14 01:13:11	832
00037884027	XRT/PC	2012-05-15 12:22:16	2012-05-15 12:39:57	1038
00037884028	XRT/PC	2012-05-16 13:53:07	2012-05-16 14:10:57	1048
00037884029	XRT/PC	2012-05-17 12:21:48	2012-05-17 12:39:56	1078
00037884030	XRT/PC	2012-05-18 23:49:33	2012-05-18 23:56:57	431
00037884031	XRT/PC	2012-05-19 20:43:36	2012-05-19 21:00:56	1028
00037884032	XRT/PC	2012-05-20 00:03:19	2012-05-20 12:59:57	1048
00037884034	XRT/PC	2012-05-22 05:06:26	2012-05-22 23:59:56	1181
00037884035	XRT/PC	2012-05-24 12:54:35	2012-05-24 13:09:55	903
00037884036	XRT/PC	2012-05-25 09:37:36	2012-05-25 09:53:56	965
00037884037	XRT/PC	2012-05-26 21:06:17	2012-05-26 21:23:58	1041
00037884038	XRT/PC	2012-05-28 11:19:46	2012-05-28 11:36:57	1028
00037884039	XRT/PC	2012-05-29 11:37:55	2012-05-29 11:55:56	1076
00037884040	XRT/PC	2012-05-30 11:20:37	2012-05-30 11:34:57	860
00037884041	XRT/PC	2012-05-31 00:32:41	2012-05-31 17:59:57	1206
00037884042	XRT/PC	2012-06-01 05:08:34	2012-06-01 23:13:57	1276
00037884043	XRT/PC	2012-06-03 03:30:45	2012-06-03 13:18:57	1437
00037884044	XRT/PC	2012-06-07 11:55:00	2012-06-07 12:13:56	1116
00037884045	XRT/PC	2012-06-08 10:16:52	2012-06-08 10:32:57	958
00037884046	XRT/PC	2012-06-10 12:07:51	2012-06-10 12:23:56	958
00037884047	XRT/PC	2012-06-11 10:33:08	2012-06-11 10:49:56	990
00037884048	XRT/PC	2012-06-12 18:33:08	2012-06-12 18:49:56	35
00037884049	XRT/PC	2012-06-13 07:15:36	2012-06-13 07:32:56	1018
00037884050	XRT/PC	2012-06-14 06:17:52	2012-06-14 12:47:57	1261
00037884051	XRT/PC	2012-06-15 09:32:58	2012-06-15 22:28:56	1048
00037884052	XRT/PC	2012-06-16 18:43:15	2012-06-16 20:55:58	1389
00037884053	XRT/PC	2012-06-17 05:58:52	2012-06-17 06:15:58	1018
00037884054	XRT/PC	2012-06-18 09:43:05	2012-06-18 09:48:56	351
00037884055	XRT/PC	2012-06-19 04:57:59	2012-06-19 22:27:57	1023
00037884056	XRT/PC	2012-06-20 20:58:53	2012-06-20 22:43:57	1146
00037884057	XRT/PC	2012-06-21 00:03:19	2012-06-21 17:59:57	306
00037884058	XRT/PC	2012-06-22 17:31:42	2012-06-22 17:47:57	970
00037884059	XRT/PC	2012-06-23 15:59:06	2012-06-23 16:15:56	1003
00037884060	XRT/PC	2012-06-24 02:06:00	2012-06-24 21:26:57	1048
00037884061	XRT/PC	2012-06-25 02:10:08	2012-06-25 08:40:56	1036
00037884062	XRT/PC	2012-06-26 01:56:11	2012-06-26 02:09:56	817
00037884063	XRT/PC	2012-06-27 21:21:33	2012-06-27 23:03:57	1116
00037884064	XRT/PC	2012-06-28 19:32:31	2012-06-28 19:48:56	963
00037884065	XRT/PC	2012-06-29 16:21:51	2012-06-29 16:37:56	945
00037884066	XRT/PC	2012-06-30 16:26:00	2012-06-30 16:41:56	953
00037884067	XRT/PC	2012-07-04 03:49:36	2012-07-04 04:06:54	1018

Table 2. continued.

Sequence	Obs/Mode	Start time (UT) (yyyy-mm-dd hh:mm:ss)	End time (UT) (yyyy-mm-dd hh:mm:ss)	Exposure (s)
00037884068	XRT/PC	2012-07-05 03:52:21	2012-07-05 04:09:48	990
00037884069	XRT/PC	2012-07-06 02:19:29	2012-07-06 02:32:54	800
00037884070	XRT/PC	2012-07-08 05:37:58	2012-07-08 05:57:54	1181
00037884071	XRT/PC	2012-07-09 18:50:41	2012-07-09 19:05:56	898
00037884072	XRT/PC	2012-07-10 13:44:54	2012-07-10 13:52:46	471
00037884073	XRT/PC	2012-07-12 14:11:08	2012-07-12 14:28:53	1061
00037884074	XRT/PC	2012-07-13 13:59:44	2012-07-13 14:14:54	893
00037884076	XRT/PC	2012-07-15 17:15:38	2012-07-15 17:34:54	1143
00037884078	XRT/PC	2012-07-18 17:30:12	2012-07-18 17:44:55	870
00037884079	XRT/PC	2012-07-19 09:23:35	2012-07-19 14:20:55	993
00037884080	XRT/PC	2012-07-20 09:32:19	2012-07-20 23:55:56	364
00037884081	XRT/PC	2012-07-22 01:30:28	2012-07-22 02:11:54	880
00037884083	XRT/PC	2012-07-26 01:49:11	2012-07-26 03:32:54	1209
00037884084	XRT/PC	2012-07-28 16:26:24	2012-07-28 16:42:54	985
00037884085	XRT/PC	2012-08-01 02:02:36	2012-08-01 02:18:54	973
00037884087	XRT/PC	2012-08-07 17:04:36	2012-08-07 17:23:55	1143
00037884088	XRT/PC	2012-08-09 15:42:19	2012-08-09 15:56:54	860
00037884089	XRT/PC	2012-08-11 07:59:36	2012-08-11 14:28:56	913